Proceedings of the ASME/BATH 2019
Symposium on Fluid Power and Motion Control
FPMC2019
October 7–9, 2019, Sarasota, FL, USA

FPMC2019-1653

MODELING, VALIDATION, AND INVESTIGATION OF AN ELECTROHYDRAULIC CRIMPING HAND TOOL

Eric D Norquist
Trade Focused Tools
Milwaukee Tool
Brookfield, WI, 53005
eric.norquist@milwaukeetool.com

Jonathon E Slightam[1]
High Consequence Automation and Robotics
Sandia National Laboratories
Albuquerque, NM, 87123
jslight@sandia.gov

Mark L Nagurka
Dept. of Mechanical Eng.
Marquette University
Milwaukee, WI, 53233
mark.nagurka@marquette.edu

ABSTRACT

Due to their high power density, hydraulic systems are increasingly adapted for human scale devices. For example, commercial and utility electricians use electrohydraulic cutting and crimping tools, rather than human powered tools, to cut and crimp wires that exceed 25mm in diameter. These tools greatly reduce worker-related fatigue and strain-type injuries. To improve electrohydraulic tool technology, there is a need to increase the number of applications from a single battery charge. This paper develops a high fidelity nonlinear lumped parameter model of an electrohydraulic crimping hand tool used by professional electricians. The eleventh-order model can predict tool performance with an average error of 6.9% and 4.4% with respect to the maximum energy consumption and crimp time, respectively. Simulation studies were conducted to investigate reducing the energy consumption of the tool. An independent parameter sweep was performed on the pump piston diameter. The gear ratio was a dependent parameter linked through the maximum motor torque. Increasing the pump piston diameter while increasing the gear ratio was shown to decrease the energy consumption of the tool during crimping applications. Simulations suggest that up to 30% energy can be saved per crimp by increasing the pump piston diameter and gear train ratio.

NOMENCLATURE

α_a	Fraction of Air
α_o	Valve Ball Contact Angle
β	Bulk Modulus
β_l	Bulk Modulus of the Liquid
η_{GT}	Gear Train Efficiency
θ_m	Motor Angular Position
θ_s	Cam Shaft Angular Position
ρ	Density
ω_m	Motor Angular Velocity
ω_s	Cam Shaft Angular Velocity
A	Flow Area
A_p	Pump Piston Area
A_{pb}	Check Valve Ball Pressure Area
A_r	Cylinder Ram Area
c_b	Check Valve Ball Dampening Coefficient
C_d	Discharge Coefficient
c_{is}	Linear Current Slope Coefficient
c_m	Motor Dampening Coefficient
c_p	Pump dampening Coefficient
c_r	Cylinder Ram Dampening
d_b	Valve Ball Diameter
d_p	Pressure Diameter of the Ball
d_{pp}	Pump Piston Diameter
d_v	Valve Orifice Diameter
e	Cam Shaft Eccentric
F_A	Application Force
i_f	Motor Field Current
I_m	Motor Inertia
i_{ml}	Linear Model Current
i_o	Linear Current Offset
K_b	Motor Back EMF Constant
k_{cv}	Check Valve Spring Coefficient
k_r	Cylinder Ram Spring Coefficient
K_T	Motor Torque Constant
L_f	Motor Field Inductance
m_b	Ball Mass
m_p	Pump Piston Mass
m_r	Cylinder Ram Mass
n	Polytropic Exponent
p	Pressure

[1] Previously affiliated with Marquette University

p_a	Atmospheric Pressure
p_c	Cylinder Pressure
p_{OR}	Oil Reservoir Pressure
p_p	Pump Pressure
p_{pmax}	Maximum Pump Pressure
Q	Flow
Q_{inlet}	Pump Inlet Check Valve Flow
Q_{outlet}	Pump Outlet Check Valve Flow
R_f	Motor Field Voltage
R_{GT}	Gear Train Ratio
T_L	Load Torque on Motor
T_m	Motor Torque
T_s	Cam Shaft Torque
V	Volume
V_f	Motor Field Voltage
V_{po}	Pump Initial Volume
x_b	Valve Ball Position
x_{bi}	Inlet Check Valve Ball Position
x_{bo}	Outlet Check Valve Ball Position
x_{cv}	Check Valve Spring Preload Length
x_p	Pump Piston Position
x_r	Cylinder Ram Position
x_{ro}	Cylinder Ram Spring Preload Length

INTRODUCTION

Fluid power systems are common on large machinery used to complete high force tasks on construction sites, agriculture, and manufacturing. These are areas that have tough working environments and require the movement of large items. Fluid power is used for high force applications due to the high-power density, specific power, force density, and specific force of fluid power systems. The benefits of fluid power have been studied in detail by the Department of Energy [1]. Historically fluid power research has focused on large scale systems [2], [3]. Recently more research has been conducted on small-scale fluid powered systems [4]. This includes robots [5], [6], artificial muscles [7], and prosthetics [8],[9].

The two major problems with traditional fluid power systems are precision of actuation and energy consumption [9]. Many small-scale tasks on construction sites require the high-power density of fluid power. Applications such as cutting, crimping, lifting, and bending are great fits for hydraulic hand tools. In addition, advances in battery and motor technology have made hydraulic systems more portable which has reduced the strain on the operator. Companies such as Milwaukee Tool, Stanley, Greenlee, and Huskie all manufacture electrohydraulic hand tools. Patents for electrohydraulic tools start around 1993 with Patent No. US 5,195,354 B2 with a Cam Crank Mechanism and Motor Driven Hydraulic Tool [10], which is battery powered.

To date, research and development on the modeling and design of electrohydraulic hand tools has not been published. This paper develops a lumped parameter model of a crimping electrohydraulic hand tool using first order principles.

TOOL DESCRIPTION

The tool modeled is the Milwaukee Tool M18™ FORCE LOGIC™ 12 Ton Crimper. This tool is used to make electrical termination connections with copper, aluminum, and steel cable. This tool was divided into 3 primary subsystems: motor and gear train, pump, and cylinder. The interactions of the subsystems are shown in Fig. 1. Subsystems in black boxes are included in the model and subsystems in white boxes are not. The power interaction between each subsystem is also shown.

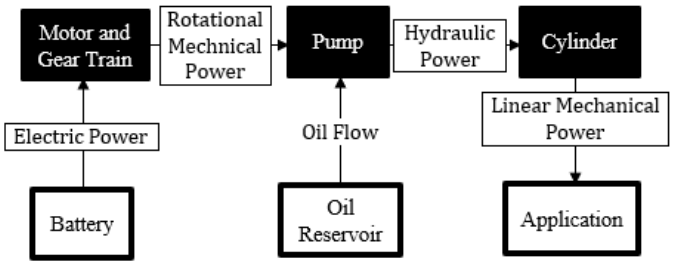

FIGURE 1: TOOL INTERACTION DIAGRAM.

The tool operates using the electrical power stored in the battery. The electric power is converted into mechanical rotational power in the motor. The rotational power is then output from the gear train. The pump converts rotational power into hydraulic power. The cylinder uses the hydraulic power to complete the application of the tool in the form of linear mechanical power.

The tool has two triggers. The upper trigger advances the ram out of the cylinder by building pressure in the cylinder. The lower trigger retracts the ram by opening a valve and reducing the pressure in the cylinder. The return valve and ram retraction are not included in the paper. The tool is shown in Fig. 2.

FIGURE 2: MILWAUKEE TOOL M18™ FORCE LOGIC™ 12 TON UTILITY CRIMPER.

During operation, the cylinder pressure is monitor by a

pressure sensor. When the cylinder pressure reaches a defined pressure, the tool electronics stop the motor. This is the primary method of how the tool regulates pressure. The tool cylinder outputs 110,000 N (24,000 lbf). The tool weighs 5.5 kg (12.2 lbf) with a Milwaukee Tool M18 CP2.0 battery.

The tool consists of a battery, motor, gear train, a positive displacement pump with two check valves, a cylinder, a pressure sensor, a return valve, and a relief valve. The tool is only modeled in the cylinder extension phase so the return valve is not included in the model. The relief valve is assumed always closed as it is only actuated if the pressure sensor fails. The relief valve is not included in the model. A schematic of the tool is shown in Fig. 3.

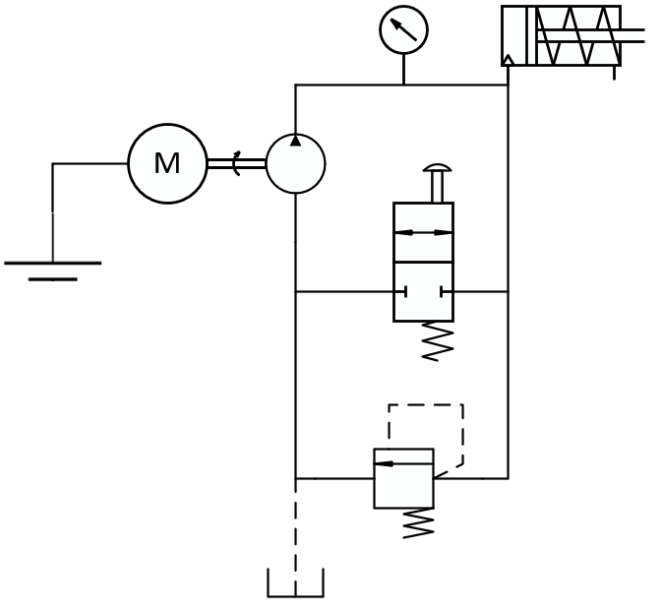

FIGURE 3: SCHEMATIC OF THE ELECTROHYDRAULIC HAND TOOL.

MODELING

The pump and cylinder of the tool were modeled using three equations: the pressure dynamics, Equation 1, the orifice equation, Equation 2, and Newton's 2nd Law. The pressure dynamics is equation is

$$\dot{p} = \frac{\beta}{V}(Q - \dot{V}), \tag{1}$$

where p is the pressure in the control volume, β is the bulk modulus of the fluid, V is the volume, and Q is the flow into the volume [11]. The orifice equation is

$$Q = AC_d\sqrt{\frac{2\Delta p}{\rho}}, \tag{2}$$

where A is the flow area, C_d is the discharge coefficient, and ρ is the fluid density. The orifice equation is used because the flow in and out of the pump is controlled by two check valves.

Motor and Gear Train Modeling

The motor in the tool is a brushless DC motor. There are many complexities involved with modeling brushless motors, such as parameters changing and saturating and the advanced controls used to control the motor [12]. Traditional brushless DC motor models could not be adapted to this system [13]. The model adopted here is a field-controlled DC motor model that replicating the performance of the tool's motor. Once model performance was correlated, the motor parameters did not change or vary.

The motor is modeled classically with electrical and mechanical subsystems, shown in Fig. 4. The two governing equations for the system are found by applying Kirchhoff's Voltage Law to the electrical circuit and Newton's 2nd Law to the mechanical system.

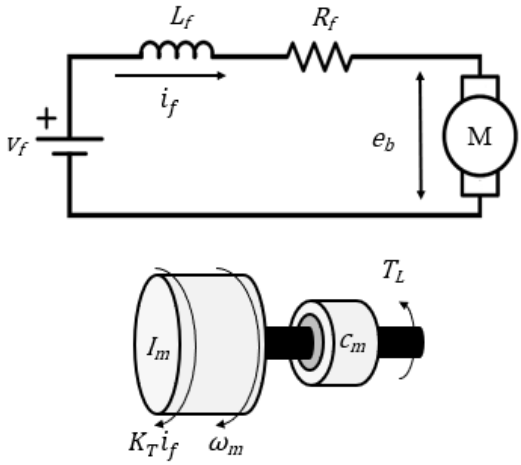

FIGURE 4: MOTOR ELECTRIC CIRCUIT AND MECHANICAL SYSTEM.

Kirchhoff's Voltage Law applied to the electrical circuit yields Equation 3.

$$\frac{di_f}{dt} = \frac{1}{L_f}\left(V_f - R_f i_f - K_b \omega_m\right) \tag{3}$$

where i_f is the field current, L_f is the field inductance, V_f is the field voltage, R_f is the field resistance, K_b is the back emf constant, and ω_m is the motor angular velocity. Newton's 2nd law applied to the mechanical system yields Equation 4.

$$\dot{\omega}_m = \frac{1}{I_m}(K_T i_f - c_m \omega_m - T_L \tag{4}$$

where I_m is the rotor inertia, K_T is the motor constant, c_m is the motor damping, and T_L is the load torque on the motor. This is a 2nd order system coupled by the field current, i_f, and motor angular velocity, ω_m.

During experimental testing it was determined that

Equations 3 and 4 could not accurately predict the motor current over a range of load torques, due to complications with the motor control software. A linear model was used to relate load torque to current.

$$i_{ml} = c_{is}T_L + i_o \tag{5}$$

where i_{ml} is the motor linear current model, c_{is} is the linear current slope constant, and i_o is the linear current model offset. One negative to this model is it will not include the inrush current seen during motor start up. Equations 3 and 4 are still used to predict the dynamic speed response of the motor.

The gear train affects the motor power by reducing the angular velocity and increasing the torque. These effects are shown in Equations 6 and 7. The output speed is proportional to the input speed. The output torque is proportional to the input torque but also includes the efficiency of the gear train.

$$\omega_m = R_{GT}\omega_S \tag{6}$$

where R_{GT} is the gear train ratio and ω_S is the cam shaft angular velocity.

$$T_m = \frac{1}{\eta_{GT}R_{GT}}T_S \tag{7}$$

where T_m is the motor torque, η_{GT} is the gear train efficiency and, T_S is the cam shaft torque.

Pump Modeling

The pump in this tool is a radial piston type positive displacement pump. Using the rotational power from the gear train, a cam shaft pushes the pump piston down to increase the pressure in the pump volume. The pump piston is coupled to the cam by a retainer. The cam, coupled through the retainer, pulls the piston out of the pump volume, lowering the pressure. Two check valves control the fluid into and out of the pump. A cross section of the pump is shown in Fig. 5. The retainer is not included in the figure.

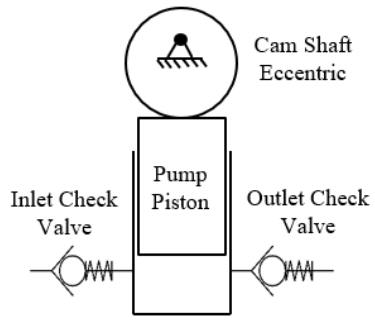

FIGURE 5: PUMP CROSS SECTION.

The pressure dynamics equation applied to the pump volume is given in Equation 8.

$$\dot{p}_p = \frac{\beta}{V_{po}A_p x_p}\left(Q_{inlet} - Q_{outlet} - A_p\dot{x}_p\right), \tag{8}$$

where p_p is the pump pressure, V_{po} is the pump initial volume, A_p is the pump piston area, x_p is the pump piston displacement, Q_{inlet} is the flow through the inlet check valve, and Q_{outlet} is the flow through the outlet check valve . These are defined as

$$Q_{inlet} = A_{Outlet}C_d\sqrt{\frac{2(p_{OR} - p_p)}{\rho}} \tag{19}$$

$$Q_{outlet} = A_{Outlet}C_d\sqrt{\frac{2(p_p - p_c)}{\rho}} \tag{20}$$

where A_{inlet} is the flow area for the inlet check valve, p_{OR} is the oil reservoir pressure, A_{outlet} is the flow area for the outlet check valve, and p_c is the cylinder pressure.

This model assumes no leakage and perfect pump efficiency. The leakage assumption is valid because the pump is sealed. The efficiency assumption will require further investigation. This is discussed in the conclusion.

The motion of the piston is found using kinematics to relate the piston to the cam shaft.

$$x_p = e - e\cos\theta_s \tag{9}$$

where e is the cam shaft eccentric and θ_s is the angular position of the cam shaft.

Newton's second law is applied to the pump piston to find the torque required to drive the pump, defined in Equation 10.

$$T_s = e[m_p e\dot{\theta}_s^2\cos(\theta_s) + c_p e\dot{\theta}_s\sin(\theta_s) + p_p A_p] \tag{10}$$

where m_p is the piston mass and c_p is the pump piston damping.

The bulk modulus of oil can be considered constant because oil is incompressible. However, oil contains 5-10% air and air is compressible. The bulk modulus of the oil and air mixture was modeled using the ideal gas equation to account for the compressibility of air [14]. This shown is in Equation 11,

$$\beta = \beta_l\frac{1+\alpha_a\left(\frac{p_a}{p_a+p}\right)^{\frac{1}{n}}}{1+\alpha_a\frac{p_a^{\frac{1}{n}}}{n(p_a+p)^{\frac{n+1}{n}}}\beta_l}, \tag{11}$$

where β_l is the bulk modulus of the liquid, α_a is the fraction of entrained air, n is the polytropic exponent of air, and p_a is atmospheric pressure.

The inlet and outlet flow of the pump is controlled by the two check valves. Figure 6 shows a cross section of the check valves used in the tool.

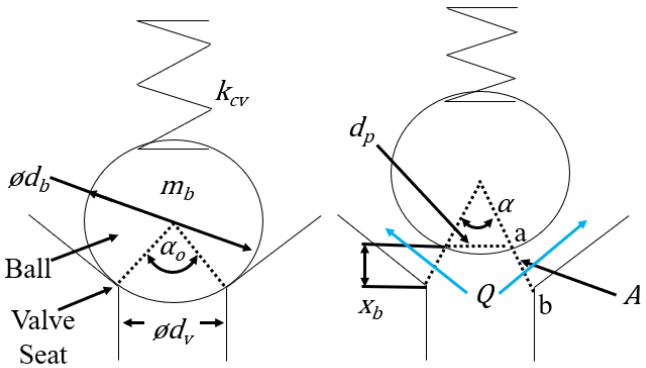

FIGURE 6: CHECK VALVE CROSS SECTION IN THE CLOSED AND OPEN POSITION.

The flow through both valves is found by using the orifice equation. The flow area is equal to the side area of a conical frustrum, given in Equation 12 [15]. This is line ab revolved on the centerline of the right section of Fig. 6,

$$A = \pi\left(\frac{d_v}{2} - \frac{d_p}{2}\right)\sqrt{\left(\frac{d_v}{2} - \frac{d_p}{2}\right)^2 + {x_b}^2}, \qquad (12)$$

where d_v is the valve orifice diameter, d_p is the pressure diameter of the ball, and x_b is the position of the ball. The position of the ball is found using Newtons 2nd Law applied to the ball.

$$\ddot{x}_b = \frac{1}{m_b}\left[\Delta p A_{pb} - c_b\dot{x}_b - k_{cv}(x_b + x_{cv})\right] \qquad (13)$$

where A_{pb} is the ball pressure area, c_b is the ball damping coefficient, k_{cv} is the check valve spring coefficient, and x_{cv} is the check valve spring preload length.

The ball pressure area, A_{pd}, is the area of a circle. The diameter of this circle is the pressure diameter, d_p. d_p is found using geometry, and is

$$d_p = d_b \sin\left(\tan^{-1}\left[\frac{d_v}{d_b\cos\left(\frac{\alpha_0}{2}\right) + 2x_b}\right]\right) \qquad (14)$$

where d_b is the ball diameter and α_o is the contact angle of the ball.

Cylinder Modeling

The tool uses a single acting spring return cylinder. The hydraulic power generated in the pump is used to extend the ram out of the cylinder. A return valve is used to drop the pressure in the cylinder and return the oil to the reservoir. The return valve is not included in this model.

The pressure in the cylinder is found using the pressure dynamics equation

$$\dot{p}_c = \frac{\beta}{A_r x_r}(Q_{outlet} - A_r\dot{x}_r) \qquad (15)$$

where A_r is the area of the cylinder ram and x_r is the cylinder ram position.

The position of the cylinder ram is found using Newton's 2nd Law

$$\ddot{x}_r = \frac{1}{m_r}\left[p_c A_r - c_r\dot{x}_r - k_r(x_r + x_{ro}) - F_A\right] \qquad (16)$$

where m_r is the mass of the ram, c_r is the damping coefficient of the ram, k_r is the cylinder spring coefficient, x_{ro} is the ram spring preload length, and F_A is the force of the application.

Comprehensive Tool Model

The subsystem models in state space form are combined to make a comprehensive tool model. This model includes the motor model, the pump model (including two check valves), and the cylinder model. The model is an eleventh order system of ordinary differential equation. The state space variables are x_1=i_f, x_2=θ_m the motor angular position, x_3=$\dot{x}_2$=ω_m, x_4=p_p, x_5=x_{bi} the inlet check valve ball position, x_6=$\dot{x}_5$, x_7=x_{bo} the outlet ball position, x_8=$\dot{x}_7$, x_9=p_c, x_{10}=x_r, and x_{11}=$\dot{x}_{10}$. Equation 17 is the input matrix for the tool model.

$$\dot{x} = \begin{Bmatrix} \frac{1}{L_f}(V_f - R_f x_1 - K_b x_3) \\ x_3 \\ \frac{1}{R_{GT} I_m}\left(K_T x_1 - c_m x_2 - \frac{T_s}{R_{GT}}\right) \\ \frac{\beta_e}{V_{po} + A_P(e - e\cos(x_2))}(\dot{V}_p + Q_{inlet} - Q_{outlet}) \\ x_6 \\ \frac{1}{m_{bi}}\left[(p_{OR} - x_4)A_{pbi} - c_{bi}x_6 - k_{cvi}(x_5 + x_{ocvi})\right] \\ x_8 \\ \frac{1}{m_{bo}}\left[(x_4 - x_9)A_{pbo} - c_{bo}x_8 - k_{cvo}(x_7 + x_{ocvo})\right] \\ \frac{\beta_e}{V_{co} + A_c x_{10}}(Q_{outlet} + A_c\dot{x}_{10}) \\ x_{11} \\ \frac{1}{m_r}\left[x_9 A_c - c_c x_{11} - k_c(x_{10} + x_{ro}) - F_A\right] \end{Bmatrix} \qquad (17)$$

where

$$T_s = e[m_p e \left(\frac{x_3}{R_{GT}}\right)^2 \cos\left(\frac{x_2}{R_{GT}}\right) + c_p e \frac{x_3}{R_{GT}} \sin\left(\frac{x_2}{R_{GT}}\right) + p_p A_p] \quad (18)$$

$$Q_{inlet} = A_{Outlet} C_d \sqrt{\frac{2(p_{OR} - x_4)}{\rho}} \quad (19)$$

$$Q_{outlet} = A_{Outlet} C_d \sqrt{\frac{2(x_4 - x_9)}{\rho}} \quad (20)$$

The output is y_1=i_{ml}. Equation 21 is the output equation.

$$y_1 = i_{mc} \frac{T_s}{R_{GT}} + i_o \quad (21)$$

MODEL VALIDATION

The model was simulated using Simulink with a stiff solver, ode15s, and variable time step. To validate the model, each subsystem was tested. The tool was also tested while completing an application. The simulation results and experimental data were compared.

Motor and Gear Train Model Validation

To validate the motor model the motor was tested in both dynamic and static conditions. Current and motor speed were monitored during both tests. During the dynamic test the motor was not subject to a load. During static testing the load on the motor was varied.

The results of the dynamic test are shown in Fig. 7 compared to the simulation results from Equations 3 and 4. The model is able to predict the dynamic motor performance during start up and at steady state. The one area without correlation is the motor slow down. The tool electronics incorporate software braking that is not included in the model.

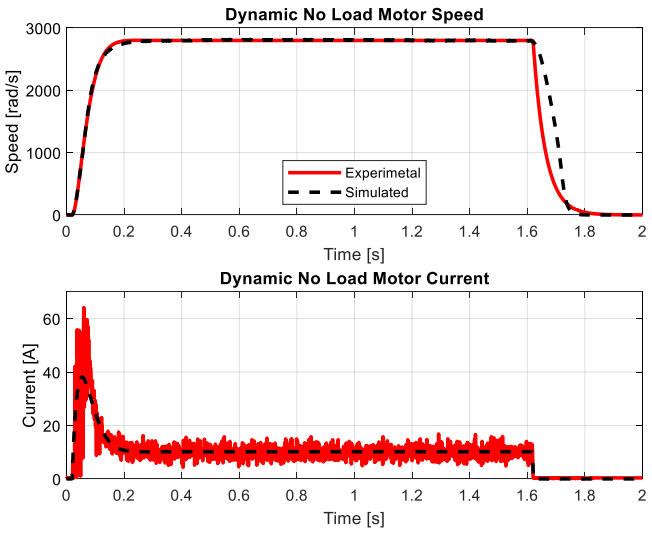

FIGURE 7: MOTOR DYNAMIC RESPONSE.

The results of the static test are shown in Fig. 8 compared to the simulation results from Equations 3-5. The speed model and linear current model are able to predict motor performance throughout the entire torque range. The dynamic current model does not correlate beyond one torque value. The linear current model, Equation 5, was used to estimate the current because the dynamic current model does predict the motors current use. The dynamic model, Equations 3 and 4, is still used to predict motor speed.

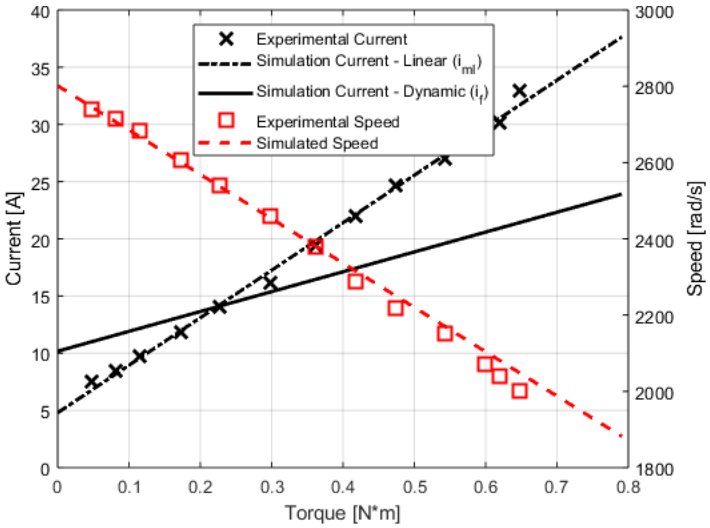

FIGURE 8: MOTOR STATIC RESPONSE.

Pump Model Validation

The pump was tested as both a closed volume and as an open volume. The closed volume test validated the pump pressure dynamics model. The pump open volume test validated the pump flow model and the check valve model.

The closed volume test consisted of cycling the pump piston in a closed volume. The piston's motion changes the pressure inside the control volume. The test was run at two different pressures, 2000 psi (140 bar) and 6000 psi (420 bar). The pressure was monitored with a pressure sensor and the pump cam shaft torque and position were monitored with a combined torque and angular position sensor. The results of the closed volume test are shown in Fig. 9.

At approximately 140 bar, the pressure oscillated between 140 bar and 15.2 bar, or a magnitude of 1.2 bar per pump revolution. At approximately 420 bar, the pressure oscillated between 400 bar and 41.8 bar, or a magnitude of 1.8 bar. The change in magnitude is due to the change in bulk modulus at different pressures. The torque oscillation magnitude also changed. At approximately 140 bar the oscillation magnitude was 2.4 N-m, compared to 6.4 N-m at approximately 420 bar. The simulation had good correlation to the experimental results.

The open volume experiment consisted of testing the flow rate of the pump at different pressures. The pump was powered using the tool motor and gear train. The load pressure of the pump was controlled using an external relief valve. The pump flow rate was monitored by capturing a known volume of fluid

for a known amount of time. The results are shown in Fig. 10. The results correlate within 8% error.

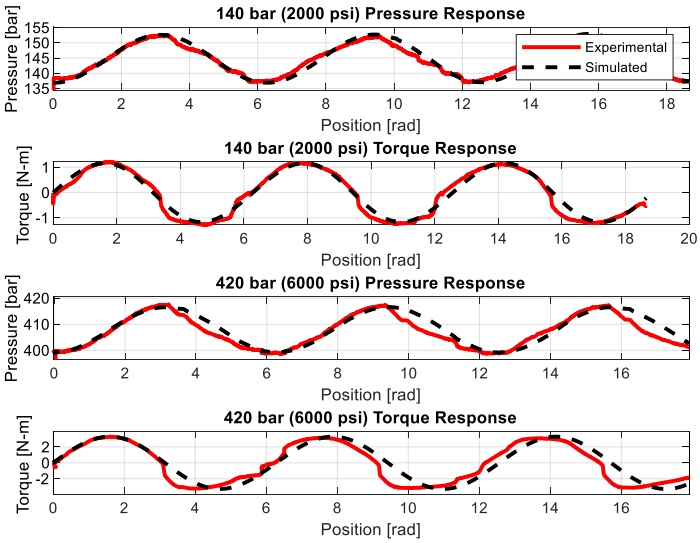

FIGURE 9: PUMP CLOSED VOLUME RESPONSE.

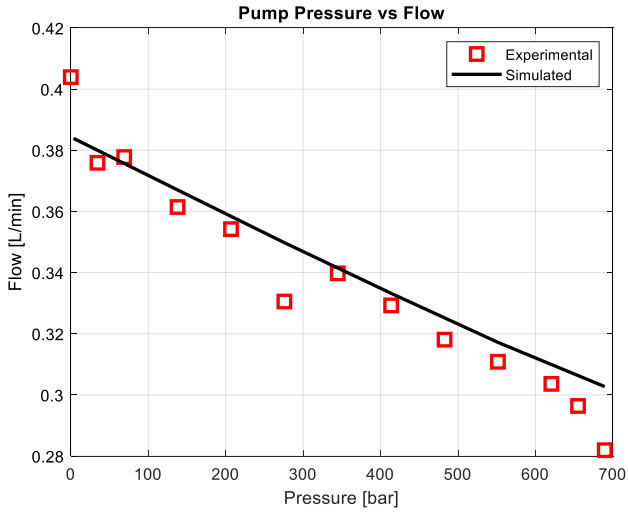

FIGURE 10: PUMP OPEN VOLUME RESPONSE.

Cylinder Model Validation

The cylinder was tested as system with motor, gear train, and pump providing the supply pressure and flow. The cylinder was run from the fully retracted state until it reached full pressure. The cylinder ram position was monitored with a string potentiometer and the pressure was monitored with a pressure sensor. The position and pressure response are shown in Fig. 11.

There are two main areas where the model does not match the experimental data. The first is at tool start up with a delay in the actual tool start up that is not included in the model. The delay is likely caused by compliance in the oil or mechanical parts.

The other area lacking correlation is the transition from low to high pressure. This occurs at approximately 4 seconds. The model had a sharp transition from low to high pressure while the experimental data shows gradual transition. The difference is likely caused by inaccuracies in the bulk modulus model at low pressures.

There is also some error involve with the no load portion of the pressure response. This is likely due to the resolution of the sensor used to gather the data. The sensor is a 700 bar sensor and the no load pressure is less than 1% of sensor range.

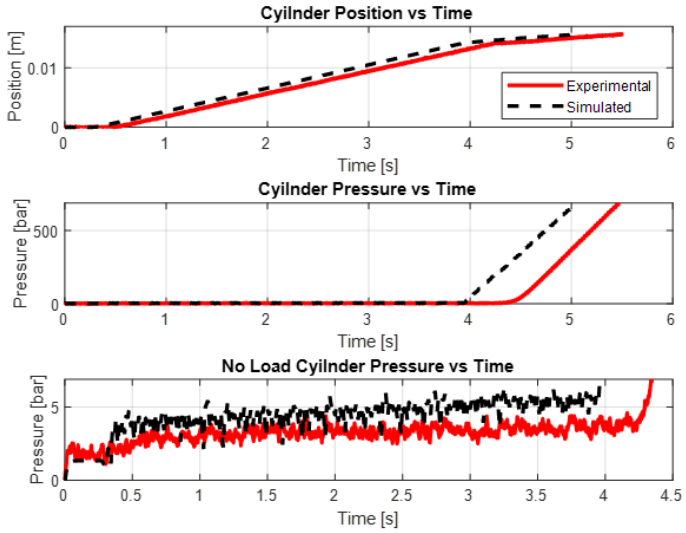

FIGURE 11: CYLINDER EXTENSION RESPONSE.

Comprehensive Tool Model Validation

The tool was tested by completing a crimp on a 750 MCM copper splice. A 750 MCM copper splice is shown in Fig. 12 and 13. This connector was selected because it requires the maximum force of the tool to complete. The cylinder ram position was monitored with a string potentiometer. The motor current was monitored with a current clamp. The motor current is converted into energy by multiplying by the battery voltage and then integrating with respect to time.

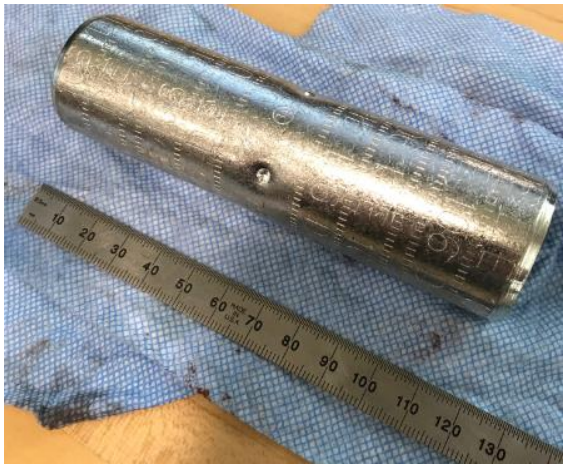

FIGURE 12: 750 MCM COPPER SPLICE BEFORE CRIMP.

FIGURE 13: 750 MCM COPPER SPLICE AFTER TWO CRIMPS.

The results are shown in Fig. 14. The error is shown in Fig. 15 and summarized in Table 1. Figure 15 was found by subtracting the experimental data from the simulated data. The same sources of error from the cylinder experiment are seen in the position response. The current response shows some initial error due to the model not including the inrush current. The largest source of error is due to the current slope not matching.

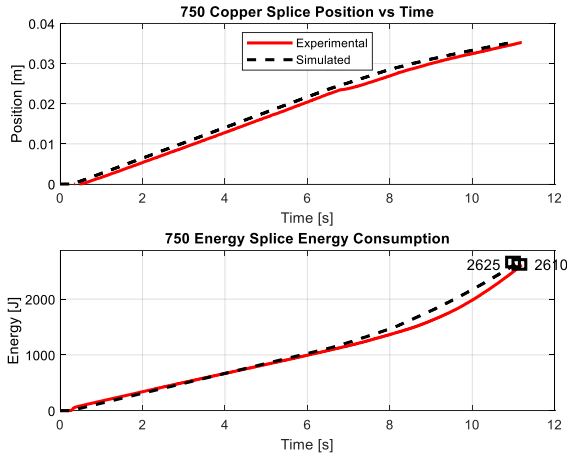

FIGURE 14: TOOL POSITION AND ENERGY RESPONSE.

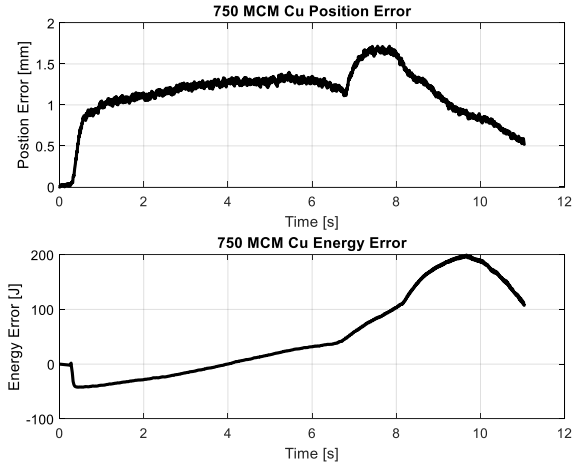

FIGURE 15: SIMULATION RESPONSE MINUS EXPERIMENTAL DATA.

Table 1: Tool Model Error Summary.

Model Output	Max |error|	Max%|error|	RMS(error)
Position	1.717 mm	4.77%	1.194 mm
Energy	199 J	7.59%	58.5 J

PARAMETER INVESTIGATION

With the established model a parameter investigation was completed. The goal of the investigation was to reduce tool energy consumption. A single independent parameter was varied. The parameter is the gear train ratio, which is linked to the pump piston diameter through the maximum torque at the motor.

The maximum torque at the motor was found using Equation 22.

$$T_m = \frac{\pi d_{pp}^2 p_{pmax} e}{4 R_{GT}} \tag{22}$$

where d_{pp} is the pump piston diameter and p_{pmax} is the maximum pump pressure and equal to 690 bar. Also, the gear train efficiency was decreased as the gear train ratio increased. This is to account for the increase in inefficiencies with a larger gear train. The gear train efficiency drops for each additional stage needed. The different values of the gear train ratio, gear train efficiency, and the pump piston diameter for each simulation are shown in Table 2.

Table 2: Parameter Investigation Simulations.

Simulation	Gear Ratio	Gear Train Efficiency [16]	Piston Diameter (mm)
Simulation 1	0.5	0.98	1.448
Simulation 2	5	0.98	4.597
Simulation 3	7.5	0.98	5.639
Simulation 4	10	0.96	6.502
Tool As Is	10.587	0.96	6.693
Simulation 5	12.5	0.96	7.264
Simulation 6	15	0.94	7.976
Simulation 7	17.5	0.94	8.611
Simulation 8	20	0.92	9.195
Simulation 9	25	0.9	10.287
Simulation 10	30	0.89	11.278

Each simulation was run while monitoring tool application time and tool energy consumption. The application time is important because changes to improve energy consumption cannot significantly increase application time. A significant increase in application time could make the tool unusable. The results of the simulations are shown in Fig. 16 and Fig. 17.

The simulations predicted that both energy consumption and

application time decrease when the great train ratio and pump piston diameter increase. The reason for this change is a reduction in average motor torque, which results in a decrease in motor current and increase in motor speed. Figure 18 compares the motor torque from the original simulation to the motor torque from simulation 8. The motor torque dropped from 0.09 N-m to 0.05 N-m.

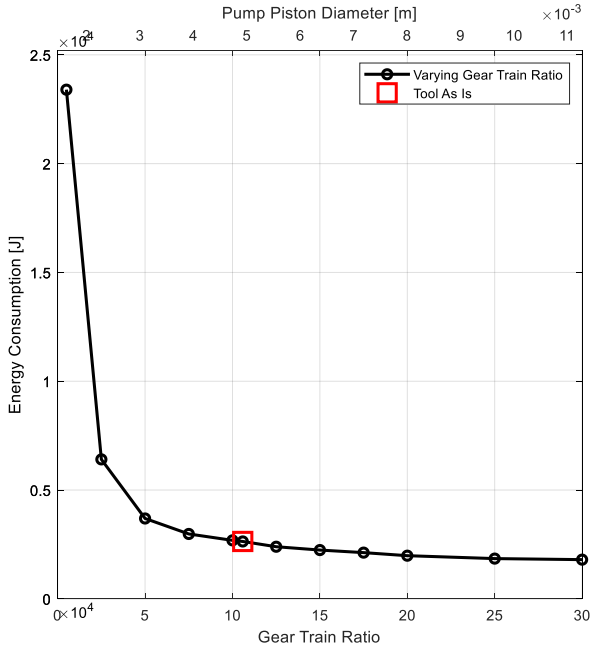

FIGURE 16: PARAMETER INVESTIGATION ENERGY CONSUMPTION SUMMARY.

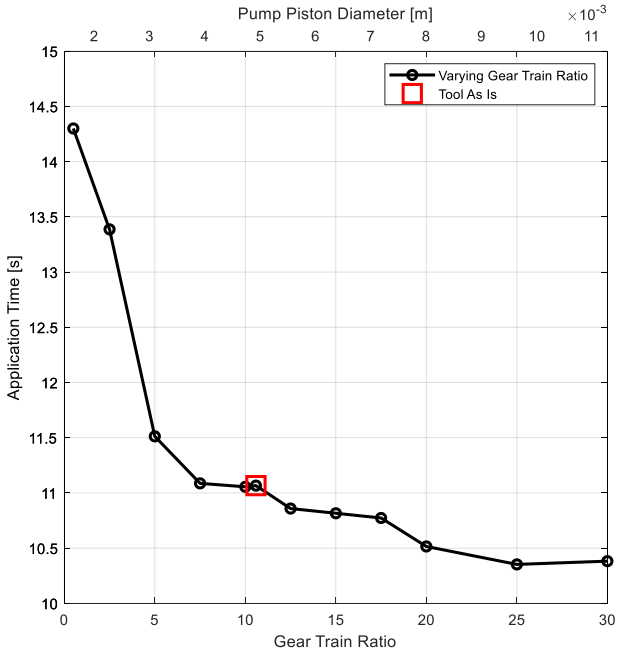

FIGURE 17: PARAMETER INVESTIGATION APPLICATION TIME SUMMARY.

The decrease in energy consumption and application time are positive effects of increasing the gear ration and pump piston diameter. A negative affect is the gear train and pump piston will have to increase in length and weight. The change in length and weight will be approximately 10mm and 0.15 kg, respectively, to achieve a 30% decrease in energy consumption.

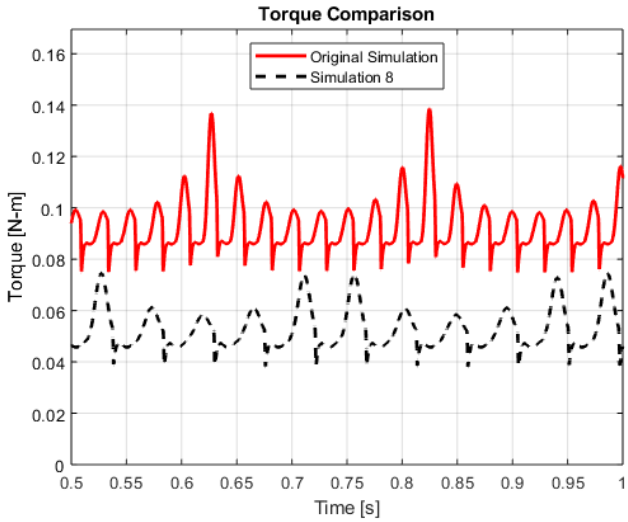

FIGURE 18: MOTOR TORQUE COMPARISON

CONCLUSION

The tool model was able to predict tool performance within 5% maximum error for ram position and 8% error for energy consumption. The major sources of error for the ram position are at tool start up and at the transition from low to high pressure. There is no one major source of error for energy consumption.

Completing a parameter investigation on the tool found that the energy consumption could be improved by increasing the gear train ratio and the pump piston diameter. A recommended design of 25 for the gear train ratio and 10.287 mm for the diameter would decrease energy consumption from 2625 J to 1850 J, or 30%. The number of applications per Milwaukee Tool M18 CP2.0 battery would increase from 49 to 70. The application time would decrease from 11.4 s to 10.4, or 9%.

Future work in this area would be to validate the performance improvements and refine the subsystems models: motor dynamic current model, bulk modulus model, flow model, and check valve model. The motor dynamic current does not predict the current over the necessary range of torque values. The bulk modulus model is unable to accurately predict the transition from low to high pressure. The flow model was inaccurate at the no load flow and max operating pressure. This could be due to not including pump efficiency.

The check valve model must be experimentally validated as a standalone subsystem before different check valve parameters can be varied. While investigating the check valve model the pump efficiency should be studied. It is likely changing the speed of the pump will affect the efficiency. Changing the check valve parameters could compensate for the change in pump efficiency.

REFERENCES

[1] Love, L., Lanke, E., Alles, P., "Estimating the Impact (Energy, Emissions and Economics) of the U.S. Fluid Power Industry" Oak Ridge National Laboratory. December, 2012.

[2] Casoli, P., Pompini N., Riccò L., 2015, "Simulation of an Excavator Hydraulic System Using Nonlinear Mathematical Models", Journal of Mechanical Engineering, 61(2015)10, 583-593, pp. 583-593.

[3] Yang S., Kwon s., Jin s,. 2008, "Hydraulic Simulation and Remote Control System of Field Robot". Intl. Conf. on Control, Automation, Robotics and Vision, December 2008.

[4] Xia, J., Durfee, W., "Analysis of Small-Scale Hydraulic Actuation Systems". ASME Journal of Mechanical Design, September 2013.

[5] Semini C., Tsagarakis N., Guglielmino E., Focchi M., Cannella F., Caldwell D., 2011, "Design of HyQ – a Hydraulically and Electrically Actuated Quadruped Robot". Institution of Mechanical Engineers Part I: J. Systems and Control Engineering, February 2011.

[6] J.Tanaka, K.Suzumori, M.Takata, T.Kanda, and M.Mori, 2005, "A Mobile Jack Robot for Rescue Operation", Proceedings of the 2005 IEEE International Workshop on Safety, Security and Rescue Robotics.

[7] Slightam, J.E., Nagurka,., 2018, "Modeling of Pneumatic Artificial Muscle with Kinetic Friction and Sliding Mode Control", Research Gate, Milwaukee, WI.

[8] Love L., Lind R., and Jansen J., 2009, "Mesofluidic Actuation for Articulated Finger and Hand Prosthetics". IEEE/RSJ International Conference on Intelligent Robots and Systems, October 2009.

[9] A. van den Bogert, S. Samorezov, B. Davis and W. Smith, "Modeling and Optimal Control of an Energy-Storing Prosthetic Knee", *Journal of Biomechanical Engineering*, vol. 134, no. 5, p. 051007, 2012.

[10] Yasui, T., Kobayashi, M., "Cam Crank Mechanism and Motor Driven Hydraulic Tool", USA, Patent Number: 5,195,354.

[11] Slightam, J.E., Nagurka,.. and Barth, "Sliding mode Impedance Control of a Hydraulic Artificial Muscle". *Proceedings of the ASME 2018 International Dynamic Systems and Control Conference,* 2018.

[12] Wackwitz, J., Principal Engineer, Milwaukee Tool, 2018.

[13] Luk P.C.K and Lee C.K,"Efficient modeling for a brushless DC motor drive,"International Conference on Industrial Electronics,Control and Instrumentation, vol.1,September 1994, pp. 188-191.

[14] MathWorks "Custom Hydraulic Fluid." MathWorks. Available: www.mathworks.com/help/physmod/hydro/ref/hydraulicfluid.html?s_tid=doc_ta. [Accessed: 06- Nov- 2018].

[15] Rabbie, M. G., "Fluid Power Engineering". Cairo, Egypt: Mc Graw Hill, 2009.

[16] Molian, S., "Mechanism Design: an Introductory Text", Cambridge University Press, 1982